Crystal Structures of Eosinophil-Derived Neurotoxin (EDN) in Complex with the Inhibitors 5′-ATP, Ap_3A, Ap_4A, and Ap_5A[†,‡]

Matthew D. Baker,[§] Daniel E. Holloway,[§] G. Jawahar Swaminathan,[§,||] and K. Ravi Acharya*[,§]

Department of Biology and Biochemistry, University of Bath, Claverton Down, Bath BA2 7AY, United Kingdom

Received September 13, 2005; Revised Manuscript Received November 4, 2005

ABSTRACT: Eosinophil-derived neurotoxin (EDN) is a catalytically proficient member of the pancreatic ribonuclease superfamily secreted along with other eosinophil granule proteins during innate host defense responses and various eosinophil-related inflammatory and allergic diseases. The ribonucleolytic activity of EDN is central to its antiviral and neurotoxic activities and possibly to other facets of its biological activity. To probe the importance of this enzymatic activity further, specific inhibitors will be of great aid. Derivatives of 5′-ADP are among the most potent inhibitors currently known. Here, we use X-ray crystallography to investigate the binding of four natural nucleotides containing this moiety. 5′-ATP binds in two alternative orientations, one occupying the B_2 subsite in a conventional manner and one being a *retro* orientation with no ordered adenosine moiety. Diadenosine triphosphate (Ap_3A) and diadenosine tetraphosphate (Ap_4A) bind with one adenine positioned at the B_2 subsite, the polyphosphate chain extending across the P_1 subsite in an ill-defined conformation, and a disordered second adenosine moiety. Diadenosine pentaphosphate (Ap_5A), the most avid inhibitor of this series, binds in a completely ordered fashion with one adenine positioned conventionally at the B_2 subsite, the polyphosphate chain occupying the P_1 and putative P_{-1} subsites, and the other adenine bound in a *retro*-like manner at the edge of the B_1 subsite. The binding mode of each of these inhibitors has features seen in previously determined structures of adenosine diphosphates. We examine the structure−affinity relationships of these inhibitors and discuss the implications for the design of improved inhibitors.

Eosinophils are leukocytes that store a battery of toxic proteins in cytoplasmic granules. These cells are recruited to tissues in response to parasitic infections, whereupon the toxic proteins are secreted as part of the innate host defense system (*1*). The granule proteins include eosinophil-derived neurotoxin (EDN;[1] RNase 2) and eosinophil cationic protein (ECP; RNase 3), two closely related members of the pancreatic ribonuclease superfamily (*2*). ECP possesses potent helminthotoxic and bactericidal activities, but those of EDN are considerably weaker (*3*, *4*). Each reduces the infectivity of respiratory syncytial virus for target cells *in vitro*, possibly mediating the antiviral activity of eosinophils against isolated virions in the respiratory tract (*5*). In addition, EDN functions as a selective chemoattractant for dendritic cells and elicits therefrom the production of a variety of soluble inflammatory mediators including cytokines, chemokines, and growth factors (*6*, *7*).

Eosinophil infiltration and degranulation are also characteristic features of allergic inflammation (*8*). Markedly elevated levels of eosinophil granule proteins including EDN and ECP have been found in the inflamed tissues of patients suffering from allergic asthma, rhinitis, inflammatory bowel disease, atopic dermatitis, and certain eye diseases (*9*−*13*), where they are believed to contribute to the symptoms. The extent of the involvement of EDN in these allergic disorders is not clear at present, but in extreme experimental models, exogenous EDN applied in high concentrations is toxic toward certain neural cell types (*14*, *15*) and hence the name of the protein.

The ribonucleolytic activity of EDN is central to its antiviral and neurotoxic activities (*5*, *16*) and possibly to other facets of its biological activity. To probe the importance of its enzymatic activity further, specific EDN inhibitors will be of great aid. At present, inhibition can be achieved with low-molecular-weight compounds (*17*) or with the naturally occurring ribonuclease inhibitor protein, RI, and derivatives thereof (*18*). The rational design of such inhibitors requires a structural understanding of the active site and adjacent regions of the enzyme. Much can be inferred from existing kinetic and crystallographic analyses of the archetypical ribonuclease, bovine pancreatic ribonuclease A (RNase A; EC 3.1.27.5) (*19*−*21*). These show that the scissile RNA phosphodiester bond and the nucleotide bases immediately up- and downstream are bound by key catalytic and specific-

[†] This work is supported by the Wellcome Trust (U.K.) through a Program Grant (067288) to K.R.A.

[‡] The atomic coordinates and structure factors for EDN in complex with 5′-ATP (codes 2C01 and R2C01SF), Ap_3A (codes 2C02 and R2C02SF), Ap_4A (codes 2C05 and R2C05SF), and Ap_5A (codes 2BZZ and R2BZZSF) have been deposited in the RCSB Protein Data Bank, www.pdb.org.

* To whom correspondence should be addressed. Telephone: +44-1225-386238. Fax: +44-1225-386779. E-mail: bsskra@bath.ac.uk.

[§] University of Bath.

[||] Present address: European Bioinformatics Institute, Wellcome Trust Genome Campus, Hinxton, Cambridge CB10 1XD, U.K.

[1] Abbreviations: EDN, eosinophil-derived neurotoxin; ECP, eosinophil cationic protein; RNaseA, bovine pancreatic ribonuclease A; Ap_nA, diadenosine 5′,5^n-P^1,P^n-polyphosphate; Ap_3A, diadenosine triphosphate; Ap_4A, diadenosine tetraphosphate; Ap_5A, diadenosine pentaphosphate; NMPK, nucleoside monophosphate kinase.

10.1021/bi0518592 CCC: $33.50
Published on Web 12/20/2005

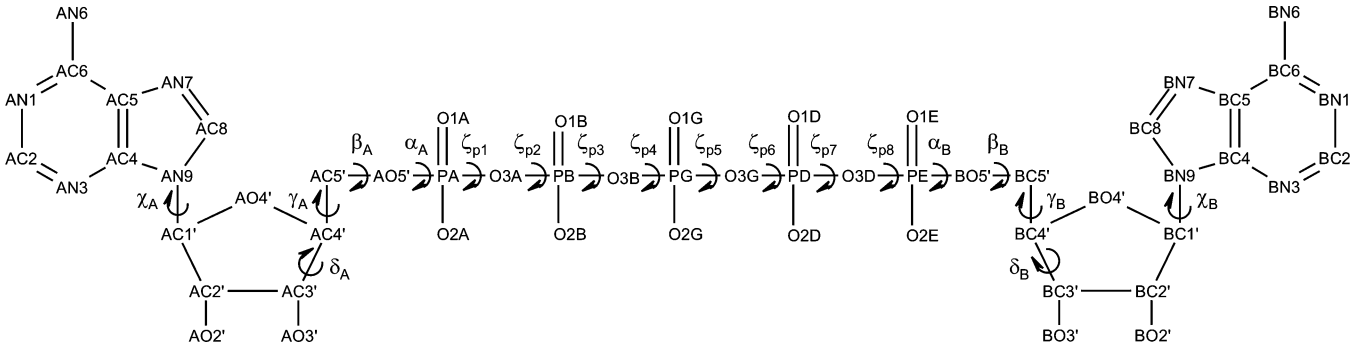

FIGURE 1: Atom-numbering and torsion-angle scheme for Ap_5A. Torsion-angle definitions follow IUPAC−IUB recommendations (*66*) where possible. Ap_4A lacks the ϵ phosphate, while Ap_3A lacks the δ and ϵ phosphates.

ity-determining subsites designated P_1, B_1, and B_2, respectively. The B_1 subsite is specific for pyrimidines, and the B_2 subsite is selective for purines. In RNase A, B_1 does not discriminate strongly between C and U (*16*, *22*), while B_2 has a 12−25-fold preference for A over G (*19*, *23*). Other peripheral subsites interact with RNA substituents further upstream (subsites P_{-1} and P_0) and downstream (subsites P_2 and B_3).

Kinetic and crystallographic analyses of EDN have provided some details of its B_1, P_1, and B_2 subsites (*16*, *22*, *24*−*26*). The catalytic triad at P_1 (His-15/Lys-38/His-129) closely resembles the corresponding part of RNase A (His-12/Lys-41/His-119), as do key specificity-determining residues at B_1 (EDN Thr-42 corresponds to RNase A Thr-45) and B_2 (EDN Asn-70 and His-129 correspond to RNase A Asn-71 and His-119). Other residues that contribute to the B_1 and B_2 subsites are less strictly conserved, and a major difference in substrate specificity occurs at B_2, where EDN has an unusually strong (500−1100-fold) preference for A over G (*22*). Three-dimensional alignment with RNase A and the observation of bound anions has also allowed the assignment of potential peripheral phosphate-binding subsites, P_{-1}, P_0, and P_2.

Adenylic mononucleotide diphosphates such as 5′-ADP (ppA) and 3′,5′-ADP are inhibitors of EDN with K_i values in the 10^{-5}−10^{-4} M range and are potential starting points for the design of tight-binding inhibitors (*25*). Recently, Kumar et al. established that several larger, naturally occurring nucleotides that incorporate the ppA structure are also inhibitors of EDN (*27*). These include 5′-ATP (pppA) and dinucleotides of the form Ap_nA (diadenosine 5′,5^n-*P*^{1},*P*^{n}-polyphosphate) such as Ap_3A, Ap_4A, and Ap_5A (Figure 1). The binding strengths of Ap_4A ($K_i = 1.9 \times 10^{-6}$ M) and Ap_5A ($K_i = 3.7 \times 10^{-7}$ M) are significantly higher than those of ppA, pppA, or Ap_3A, and the reasons for this are not obvious. Here, we report crystal structures of EDN in complex with 5′-ATP, Ap_3A, Ap_4A, and Ap_5A. They reveal how the extension of the ppA core outward from the β phosphate affects the mode of binding and suggest how improved inhibitors may be generated.

EXPERIMENTAL PROCEDURES

Protein Purification, Crystallization, and X-ray Data Collection. Recombinant EDN, expressed in *Escherichia coli* from a synthetic gene cloned into pET-11c and purified from inclusion bodies as described for ECP (*28*), was the kind gift of Dr. R. J. Youle (NIH, Bethesda, MD). The recombinant protein differs from the natural protein in that it is not glycosylated and it has an additional Met residue at the N terminus. Crystals were grown in sodium acetate at pH 6.5 using the hanging drop-vapor diffusion method as described previously (*26*). Nucleotides were introduced by soaking crystals in reservoir solution supplemented with 100 mM nucleotide (sodium salt; Sigma Chemical Co.) for 24 h. Crystals were then transferred briefly to a cryoprotectant composed of reservoir solution supplemented with 25% glycerol before collection of diffraction data at 100 K. Several preliminary data sets were collected at beamline X11 of DESY, EMBL-Hamburg, Germany. Then, data from a crystal soaked in 5′-ATP were collected using an ADSC Quantum-4 CCD detector at station PX9.6 of the SRS, Daresbury, U.K. Data from crystals soaked in Ap_3A and Ap_4A were collected using a MAR 300 image plate mounted on an Rigaku RU-H3R rotating anode source emitting Cu Kα radiation. Data from a crystal soaked in Ap_5A were collected using an ADSC Quantum-4 CCD detector at station PX14.2 of the SRS, Daresbury, U.K. All data were processed and scaled using the HKL suite (*29*). Data collection statistics are shown in Table 1.

Phase Determination and Refinement. Molecular replacement was performed with MOLREP (*30*, *31*) using PDB entry 1GQV (*26*) as a search model. Refinement was then conducted using CNS (*32*) with 5% of the reflections set aside for cross-validation (*33*). After one initial round of rigid-body refinement, cycles of minimization, individual *B*-factor refinement, simulated annealing, and electron-density map calculation were interspersed with manual model building using O (*34*). Ligands were added manually after one full cycle of refinement according to the density present in $F_o - F_c$ electron-density maps, and water molecules were added automatically (minimum $F_o - F_c$ peak height $= 3\sigma$). All data were included in the final round of refinement.

The EDN·Ap_5A structure was refined additionally using SHELX 97-2 (*35*). Three rounds of refinement with isotropic displacement parameters preceded multiple rounds of refinement with anisotropic displacement parameters, each of which consisted of 10 cycles of restrained CGLS refinement followed by electron-density map calculation and manual model building using O. The occupancy of all water molecules was fixed at 1.0. Alternate conformations were assigned to Phe-5, Asn-25, Gln-34, Val-51, Asn-53, Thr-67, Ser-76, Ile-81, Gln-100, Val-109, and Asn-113.

Table 1: Data Collection and Processing Statistics

	EDN·5′-ATP	EDN·Ap_3A	EDN·Ap_4A	EDN·Ap_5A
wavelength (Å)	0.979	1.54	1.54	0.979
space group	$P2_12_12_1$	$P2_12_12_1$	$P2_12_12_1$	$P2_12_12_1$
unit cell dimensions				
a (Å)	52.70	52.70	52.42	53.04
b (Å)	56.71	56.37	56.53	56.96
c (Å)	41.97	41.73	41.62	42.26
resolution range	40.0−1.24	20.0−2.00	20.0−1.86	40.0−0.98
number of reflections				
measured	366 963	32 823	75 292	601 614
unique	36 418	8785	10 540	74 196
R_{symm}[a]	0.049 (0.134)	0.080 (0.325)	0.076 (0.392)	0.076 (0.136)
$I/\sigma(I)$	32.1 (13.7)	12.2 (3.1)	16.5 (2.7)	23.1 (11.1)
completeness (%)	99.1 (100)	99.2 (99.1)	96.8 (95.9)	94.4 (91.2)

[a] $R_{symm} = \sum_h\sum_i [|I_i(h) - \langle I(h)\rangle|/\sum_h\sum_i I_i(h)]$, where I_i is the *i*th measurement and $\langle I(h)\rangle$ is the weighted mean of all of the measurements of $I(h)$. Figures in parentheses refer to the highest resolution shell (1.28−1.24, 2.07−2.00, 1.93−1.86, and 1.02−0.98 Å for EDN·5′-ATP, EDN·Ap_3A, EDN·Ap_4A, and EDN·Ap_5A, respectively).

Table 2: Refinement Statistics

	EDN·5′-ATP	EDN·Ap_3A	EDN·Ap_4A	EDN·Ap_5A
resolution (Å)	1.24	2.00	1.86	0.98
number of non-hydrogen atoms				
protein	1099[a]	1089	1089	1137[a]
water	192	105	117	210
acetate	4	4	4	4
nucleotide	36[a]	27	31	57
R_{cryst}[b]	0.188	0.190	0.185	0.134
R_{free}[c]	0.221	0.228	0.215	0.162
goodness of fit[d]				2.74
deviation from ideality (rms)				
bond lengths (Å)	0.004	0.006	0.006	0.007
bond angles (deg)	1.36	1.37	1.39	0.18
mean *B* factor by atom type				
protein	10.6	21.9	23.6	10.6[e]
water	25.0	29.2	31.6	23.0[e]
acetate	10.3	16.2	19.6	10.7[e]
nucleotide	22.1	63.0	61.0	15.3[e]

[a] Includes atoms in alternate conformations. [b] $R_{cryst} = \sum_h|F_o - F_c|/\sum_h F_o$, where F_o and F_c are the observed and calculated structure-factor amplitudes of reflection *h*. [c] R_{free} is equal to R_{cryst} for a randomly selected 5% of the reflections not used in the refinement (*33*). [d] After anisotropic refinement. [e] Mean isotropic equivalent *B* factor.

Distribution of anisotropy was monitored using PARVATI (*36*); those residues identified as having extreme anisotropy were refined isotropically thereafter. In the final round of refinement, the positions of riding hydrogen atoms were calculated for all residues apart from those in alternate conformations and those excluded from anisotropic refinement. Refinement statistics are given in Table 2.

Final structures were analyzed using PROCHECK (*37*), BAVERAGE, SUPERPOSE, and GEOMCALC from the CCP4 suite (*31*) and HBPLUS (*38*). The accessibility and presence of clefts and crevices on the protein surface were assessed using VOIDOO (*39*).

RESULTS

Topology and Gross Features. The crystal structures of EDN in complex with 5′-ATP, Ap_3A, Ap_4A, and Ap_5A were determined at resolutions of 1.24, 2.00, 1.86, and 0.98 Å, respectively. Each structure contains all 135 amino acid residues plus one nucleotide. In their respective Ramachandran plots, 89−90% of the residues lie in the most favorable regions and none lie in disallowed regions. Main-chain electron density is continuous apart from at the extreme N and C termini and the 89−94 loop. Disorder of the 89−94 loop or its equivalent is a characteristic of crystal structures of EDN (*24*−*26*) and other members of the pancreatic ribonuclease superfamily (*40*, *41*).

The C^α traces of the four structures are very similar, exhibiting root-mean-square (rms) deviations of 0.32−0.36 Å from the C^α trace of nucleotide-free EDN (PDB entry 1GQV) (*26*) and indicating that no major main-chain adjustments take place upon inhibitor binding. Residues 1, 66−68, 77, and 87−96 show the greatest deviation from their counterparts in 1GQV, but even these show only a modest deviation (maximum deviation = 1.2 Å for residue 90). Indeed, when they are eliminated from calculations, the C^α rms deviation drops only slightly, to 0.29 Å in each case. Furthermore, all of these outliers are located in flexible loops and do not appear to play any role in inhibitor binding.

In the following analyses, the adenine moiety bound to the B_2 site is designated "A" and the phosphate group attached directly to ribose A is designated "α" (Figure 1).

Structure of EDN·5′-ATP. Analysis of the binding of 5′-ADP, 2′,5′-ADP, and 3′,5′-ADP to EDN does not enable one to predict with confidence the mode in which 5′-ATP might bind; depending upon where the phosphate groups are attached, markedly different modes of ligand binding are observed (*25*). For example, whereas 3′,5′-ADP (a moiety

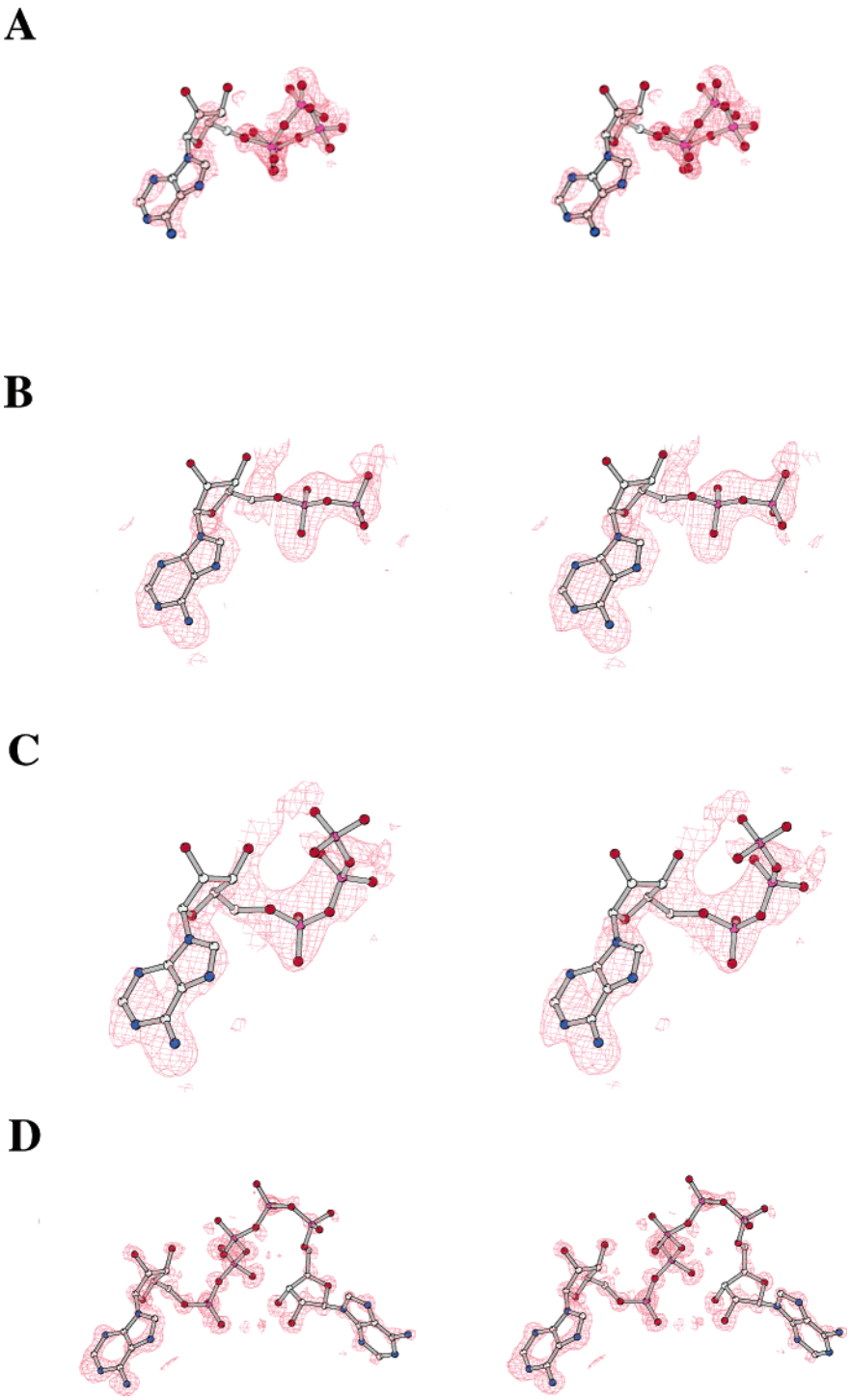

FIGURE 2: Electron-density maps for the nucleotide inhibitors. (A) 5′-ATP, (B) Ap_3A, (C) Ap_4A, and (D) Ap_5A. In each panel, the sigma A-weighted $F_o - F_c$ omit electron-density map is shown in stereo, contoured at 2.0, 2.7, 2.7, and 3σ, respectively.

found naturally in RNA) binds conventionally with its adenine at the B_2 subsite and its α phosphate at P_1 (His-129 in conformation A), 5′-ADP (ppA) binds in an unconventional, *retro*-like mode (*42*) with its adenine in the vicinity of B_1 and its β phosphate at P_1 (His-129 in conformation B). Extension of any attached polyphosphate chain (with its inherent torsional flexibility) might even further increase the number of phosphate-binding permutations at the P_1 subsite.

The electron-density map of the EDN·5′-ATP complex indicates two modes of ligand binding (Figure 2A). It shows strong (4.5σ) density at the P_1 subsite, consistent with the binding of a diphosphate moiety in two overlapping orientations, and somewhat weaker (2.3σ) density at the B_2 subsite corresponding to an adenine moiety. No ribose density is evident. It appears that only one of the diphosphate orientations (designated "A") is associated with the adenine density and that the other ("B") has no associated adenosine density. The two orientations of the diphosphate moiety correlate with alternate conformations of the His-129 side chain [designated likewise in accordance with the two conformations observed previously in various structures of pancreatic ribonuclease superfamily members (*25*, *43*)].

In orientation A (occupancy 0.35), the interactions between the adenine and the protein can be discerned reasonably well

Table 3: Potential Hydrogen Bonds[a] between EDN and the Nucleotide Inhibitors

	length (Å)				
	EDN·5′-ATP				
donor−acceptor	orientation A	orientation B	EDN·Ap_3A	EDN·Ap_4A	EDN·Ap_5A
adenine A					
Asn-70 $N^{\delta 2}$−AN1	2.9	*b*	2.9	2.9	2.9
AN6−Asn-70 $O^{\delta 1}$	3.1	*b*	3.2	3.1	2.9
ribose A					
His-129 $N^{\delta 1}$−AO5′	*c*	*b*	*c*	*c*	3.0
α phosphate					
His-15 $N^{\epsilon 2}$−O1A	2.4	*b*	*c*	*c*	2.8
His-129A $N^{\delta 1}$−O2A	2.4	*b*	*c*	*c*	3.0
Leu-130 N−O2A	2.8	*b*	*c*	*c*	3.0
β phosphate					
Lys-38 N^{ζ}−O1B	2.7	2.8	*c*	*c*	2.7
Gln-14 $N^{\epsilon 2}$−O2B	2.9		*c*	*c*	3.0
γ phosphate					
His-15 $N^{\epsilon 2}$−O1G	*b*	3.1	*b*	*b*	
His-129B $N^{\delta 1}$−O3G	*b*	2.8	*b*	*b*	
Leu-130 N−O2G	*b*	2.8	*b*	*b*	
δ phosphate					
Arg-36 NH1−O1D	*d*	*d*	*d*	*d*	3.0

[a] Potential hydrogen bonds were identified with HBPLUS (*38*) and have H···A distances of <2.5 Å and D−H···A angles of >90°. [b] Ligand atoms that are not observed. [c] The conformation of the ligand is unclear. [d] No equivalent inhibitor atom is present.

Table 4: Hydrophobic Interactions[a] between EDN and the Nucleotide Inhibitors

	EDN atoms			
inhibitor atom	EDN·5′-ATP[b]	EDN·Ap_3A	EDN·Ap_4A	EDN·Ap_5A
adenine A				
AC2	Val-128($C^{\gamma 2}$)	Val-128 ($C^{\gamma 2}$)	Val-128 ($C^{\gamma 2}$)	Val-128 ($C^{\gamma 2}$)
AC4		His-129 (C^{β})		His-129 (C^{β}, C^{γ})
AC5				His-129 (C^{γ}, $C^{\epsilon 1}$)
AC6	Ala-110 (C^{β})	Ala-110 (C^{β})	Ala-110 (C^{β})	Ala-110 (C^{β})
AC8	His-129 (C^{γ}, $C^{\delta 2}$, $C^{\epsilon 1}$)	His-129 (C^{γ}, $C^{\delta 2}$, $C^{\epsilon 1}$)	His-129 (C^{γ}, $C^{\delta 2}$, $C^{\epsilon 1}$)	His-129 (C^{γ}, $C^{\delta 2}$, $C^{\epsilon 1}$)
ribose A				
AC4′	*c*	*c*	*c*	Trp-7 ($C^{\zeta 3}$)
ribose B				
BC5′	*d*	*e*	*e*	Lys-38 (C^{ϵ})
adenine B				
BC2	*d*	*e*	*e*	His-82 ($C^{\epsilon 1}$), Ile-133 ($C^{\gamma 1}$, $C^{\delta 1}$)
BC4	*d*	*e*	*e*	Gln-40 (C^{δ})
BC5	*d*	*e*	*e*	Gln-40 (C^{δ})
BC8	*d*	*e*	*e*	Gln-40 (C^{δ})

[a] Interactions were identified with HBPLUS (*38*). The listed atoms are ≤3.9 Å apart. [b] The ligand in orientation A. [c] The conformation of the ribose moiety is unclear. [d] Atoms that are not present in the inhibitor. [e] The electron density for adenine B and ribose B is not observed.

(Tables 3 and 4): the base engages in hydrogen bonds with Asn-70, van der Waals interactions with the side chains of Ala-110 and Val-128, and $\pi-\pi$ stacking interactions with the side chain of His-129, which adopts the active "A" conformation ($\chi_1 = 175°$, $\chi_2 = -69°$). These interactions are highly similar to those in the EDN·3′,5′-ADP complex (PDB entry 1HI4) (*25*) and in structures of adenylic nucleotide inhibitors bound productively to the B_2 subsite of RNase A (*44*−*47*). The lack of electron density prevents the conformation and interactions of the ribose moiety from being discerned with confidence. The α phosphate forms hydrogen bonds at the P_1 subsite with the side chains of His-15 and His-129 and with the main-chain nitrogen of Leu-130. The β phosphate lies within hydrogen-bonding distance of the other P_1 subsite residues, Gln-14 and Lys-38, and thus, the α and β phosphate share occupation of the P_1 subsite. In contrast, the γ phosphate appears to be in no fixed conformation and to make no contact with the protein.

In orientation B (occupancy 0.65), only a diphosphate moiety is visible. Its location and its interactions with His-129 indicate that it comprises the terminal (γ and β) phosphates of the ligand, while the α phosphate and adenosine portion are in no fixed conformation. Despite the contrasting behavior of the adenosine, this is suggestive of the *retro*-like binding mode observed in the EDN·5′-ADP structure (PDB entry 1HI5) (*25*); i.e., the polyphosphate chain runs across the P_1 subsite in a direction opposite to that of orientation A. The γ phosphate is in a position similar but not identical to that of the α phosphate of orientation A, while the β phosphates of the two orientations are in the same general position, diverging by ≈40°. Significantly, the γ phosphate engages in a hydrogen bond with the inactive "B" conformation of His-129 ($\chi_1 = 165°$, $\chi_2 = -119°$), which can only exist when the B_2 subsite is vacant. The other protein atoms with which the γ phosphate makes hydrogen bonds match those contacted by the α phosphate of orienta-

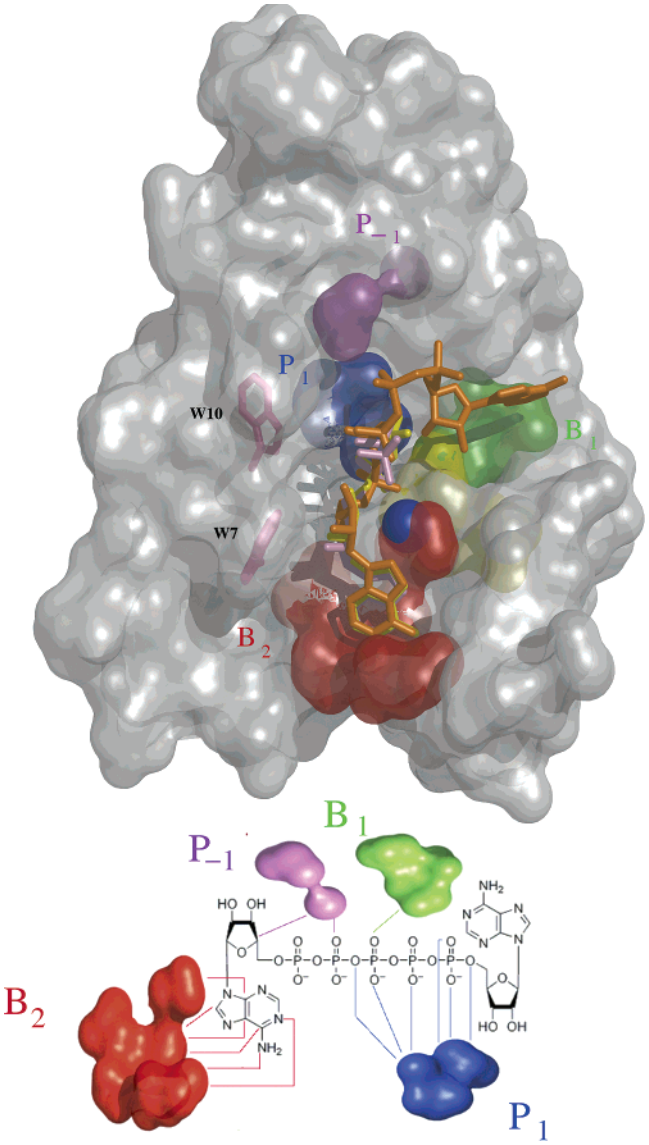

FIGURE 3: Topology of the inhibitor-binding cleft. The protein surface from the EDN·Ap_5A structure is shown with inhibitors superposed in ball-and-stick representation. The substrate-binding subsites P_{-1}, B_1, P_1, and B_2 are colored purple, green, blue, and red, respectively, while the small nonpolar cleft formed by residues Leu-45, Tyr-108, and Leu-130 (immediately next to the B_1 site) is colored yellow. Ap_3A, Ap_4A, and Ap_5A are shown in yellow, pink, and orange, respectively. Residues Trp-7 and Trp-10, which overhang the polyphosphate-binding region, are also shown in ball-and-stick representation.

tion A, while the β phosphate makes a hydrogen bond with Lys-38 but not with Gln-14.

Structures of EDN·Ap_3A and EDN·Ap_4A. With the EDN·Ap_3A and EDN·Ap_4A complexes, the electron-density map permits satisfactory modeling of adenine A but only rough modeling of ribose A and the polyphosphate chain out to the β phosphate (EDN·Ap_3A) or the γ phosphate (EDN·Ap_4A) (parts B and C of Figure 2). Because of a complete lack of electron density, it is not possible to model any part of adenosine B, and this moiety is deduced to be in no fixed conformation.

The visible portions of Ap_3A and Ap_4A bind within the active-site cleft, with adenine A positioned at the B_2 subsite and the polyphosphate chain extending across the P_1 subsite to the fringe of B_1 (Figure 3). In each case, the interactions

Table 5: Conformation of Ap_5A When Bound to EDN

	torsion angles (deg)[a]
N-glycosidic bond	
AO4′−AC1′−AN9−AC4 (χ_A)	−77 (*anti*)
backbone[b]	
AC5′−AC4′−AC3′−AO3′ (δ_A)	78 (+*sc*)
AO5′−AC5′−AC4′−AC3′ (γ_A)	58 (+*sc*)
PA−AO5′−AC5′−AC4′ (β_A)	−146 (−*ac*)
O3A−PA−AO5′−AC5′ (α_A)	65 (+*sc*)
PB−O3A−PA−AO5′ (ζ_{p1})	−76
O3B−PB−O3A−PA (ζ_{p2})	142
PG−O3B−PB−O3A (ζ_{p3})	−78
O3G−PG−O3B−PB (ζ_{p4})	−169
PD−O3G−PG−O3B (ζ_{p5})	72
O3D−PD−O3G−PG (ζ_{p6})	−157
PE−O3D−PD−O3G (ζ_{p7})	111
BO5′−PE−O3D−PD (ζ_{p8})	−64
O3D−PE−BO5′−BC5′ (α_B)	77 (+*sc*)
PE−BO5′−BC5′−BC4′ (β_B)	160 (*ap*)
BO5′−BC5′−BC4′−BC3′ (γ_B)	38 (+*sc*)
BC5′−BC4′−BC3′−BO3′ (δ_B)	136 (+*ac*)
N-glycosidic bond	
BO4′−BC1′−BN9−BC4 (χ_B)	−107 (*anti*)
ribose A pucker	
pseudorotation phase angle (deg)[c]	38
conformation	C4′-*exo*
ribose B pucker	
pseudorotation phase angle (deg)[c]	144
conformation	C2′-*endo*

[a] Torsion-angle definitions follow IUPAC−IUB recommendations (*66*) where possible. [b] Backbone torsion angles are listed in sequence from adenine A to adenine B as illustrated in Figure 1. [c] As described by Altona and Sandaralingam (*67*).

between adenine A and the protein can be discerned clearly and are essentially the same as those described above for the EDN·5′-ATP complex, orientation A (Tables 3 and 4). His-129 is exclusively in conformation A. Weak electron density prevents the conformation and interactions of ribose A from being discerned with confidence, while the likely presence of multiple conformations significantly impedes analysis of the polyphosphate chain. However, it appears likely that the α and β phosphates of each nucleotide interact with the protein.

Structure of EDN·Ap_5A. The electron-density map permits the modeling of the entire Ap_5A molecule in the EDN·Ap_5A complex (Figure 2D). As observed for the binding of Ap_3A and Ap_4A, adenine A occupies the B_2 subsite and the polyphosphate linker passes over the P_1 subsite. However, in contrast to the shorter homologues, the linker adopts a fixed conformation and adenine B resides at the edge of the B_1 subsite (Figure 3). Because of the higher resolution of the structure and the higher structural order of this nucleotide, the enzyme·inhibitor interactions can be defined more clearly (Tables 3 and 4), as can the conformation of the inhibitor (Table 5).

Adenine A interacts with EDN in a manner similar to that seen in the EDN·3′,5′-ADP, EDN·5′-ATP (orientation A), EDN·Ap_3A, and EDN·Ap_4A complexes, with the adjacent ribose making a hydrogen bond with His-129 and van der Waals interactions with Trp-7 (Figure 4). As for orientation A of the EDN·5′-ATP complex, the α phosphate forms hydrogen bonds with His-15, His-129, and Leu-130, while the β phosphate interacts with the side chains of Gln-14 and Lys-38, with all of these residues being components of the P_1 subsite. The polyphosphate chain adopts a remarkably

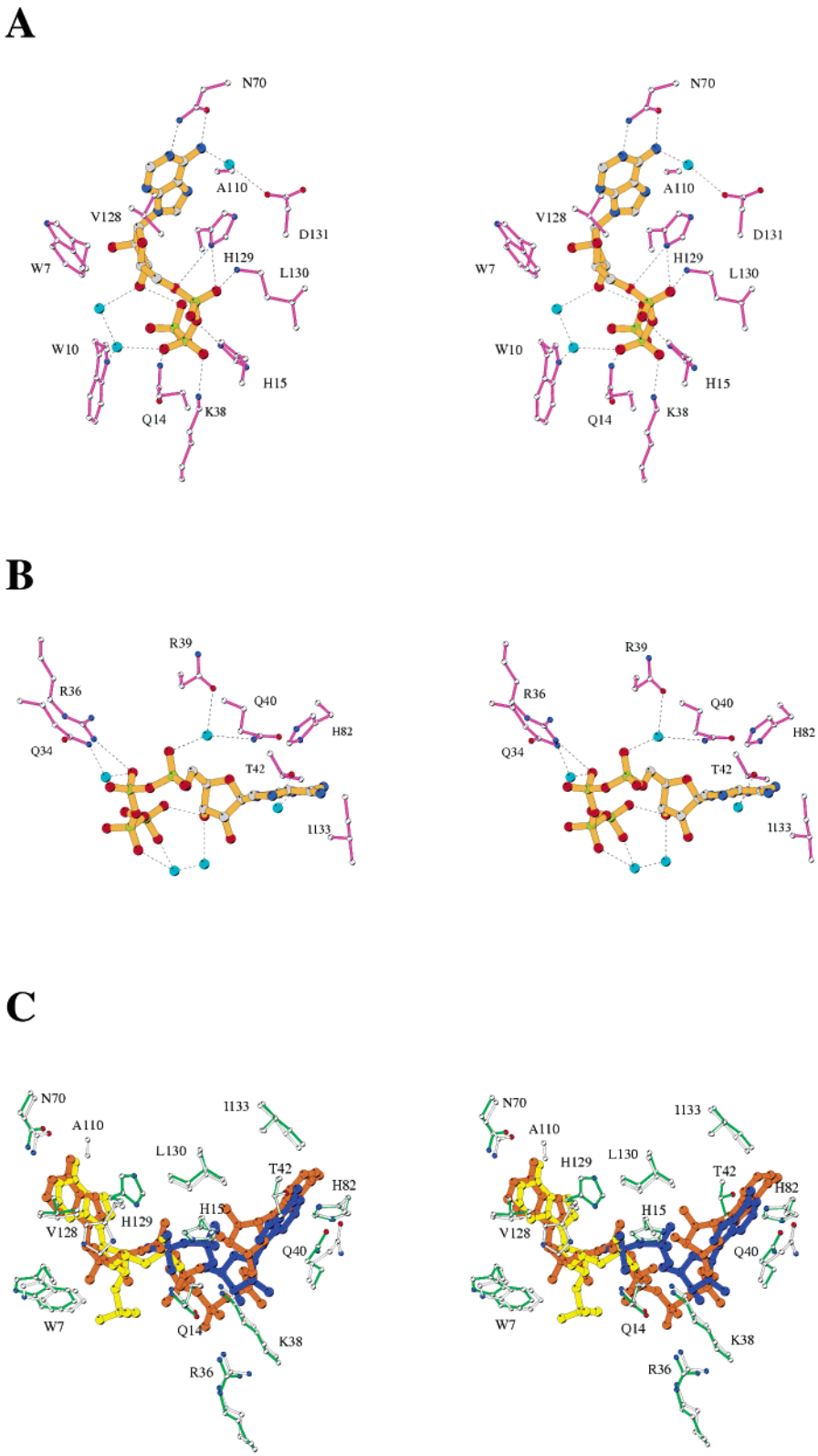

FIGURE 4: Structural details of the EDN·Ap_5A complex. (A) Adenosine A and the α, β, and γ phosphates. (B) Adenosine B and the β, γ, δ, and ϵ phosphates. Stereo ball-and-stick representations are shown, in which the inhibitor is drawn with orange sticks, protein residues are drawn with purple sticks, and selected water molecules are drawn as cyan spheres. All direct and selected water-mediated hydrogen bonds between the inhibitor and the protein are shown as dashed lines. Carbon, nitrogen, oxygen, and phosphorus atoms are colored white, blue, red, and yellow, respectively. (C) Comparison of the binding of Ap_5A, 3′,5′-ADP, and 5′-ATP to EDN. A ball-and-stick representation is shown in which the EDN·Ap_5A (orange), EDN·3′,5′-ADP (PDB entry 1HI4) (*25*) (yellow), and EDN·5′-ADP (PDB entry 1HI5) (*25*) (blue) complexes are superposed in stereo. Key protein residues from the EDN·Ap_5A structure are drawn with green sticks, while the corresponding residues from the EDN·3′,5′-ADP structure are drawn with white sticks. Carbon, nitrogen, and oxygen atoms of the protein are colored white, blue, and red, respectively.

contorted, S-shaped conformation that brings the δ phosphate within hydrogen-bonding distance of Arg-36, a potential component of the P_{-1} subsite (Figure 4) (*24*). This conformation of the polyphosphate chain is also stabilized by two

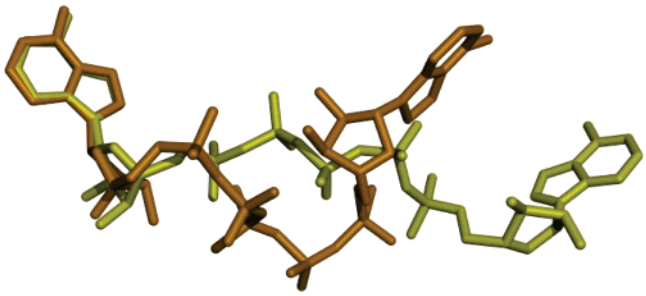

FIGURE 5: Comparison of the EDN- and adenylate kinase-bound conformations of Ap_5A. The EDN-bound conformation of Ap_5A is shown in orange, and the 1.60 Å resolution *B. stearothermophilus* adenylate kinase-bound conformation (PDB entry 1ZIN) (*58*) is shown in yellow. The adenine A rings of the two nucleotides are superposed.

internal hydrogen bonds, one between atoms AO3′ (ribose A) and O1G (γ phosphate) and one between atoms BO3′ (ribose B) and O1B (β phosphate). Ribose B makes a single van der Waals interaction with the protein at Lys-38, while adenine B stacks against the side-chain amide group of Gln-40 and makes additional hydrophobic interactions with the side chains of His-82 and Ile-133. A total of 19 water molecules are discernible within hydrogen-bonding distance of the nucleotide.

Adenine B partially blocks the pyrimidine-specific B_1 subsite. Although at present there are no crystal structures of EDN·pyrimidine nucleotide complexes available for comparison, the B_1 subsite of its relative RNase A has been well-characterized. In this enzyme, B_1 is a narrow pocket whose primary functional component is Thr-45. This residue recognizes pyrimidines via two hydrogen bonds made with atoms in the pyrimidine ring, its main-chain NH group donating a proton to the 2-keto group of either base, and its side-chain OH group donating to the N3 atom of cytidine or accepting from the N3 atom of uridine (*19*). In the EDN·Ap_5A structure, adenine B does not penetrate the putative B_1 pocket, but there is a water-mediated hydrogen bond between its N3 atom and the side-chain OH group of Thr-42, the counterpart of RNase A Thr-45 (Figure 4). This arrangement bears some resemblance to the nonproductive *retro* binding of various purine-containing nucleotides to the B_1 subsites of RNase A and bovine seminal RNase (*42*, *48*−*53*). In these cases, the purine penetrates far enough into the B_1 pocket to engage in a direct hydrogen bond with the B_1 threonine residue. Hence, the binding of adenine B of Ap_5A can be viewed as a less invasive version of this. Features of *retro* binding are also present in the EDN·5′-ADP complex (*25*), in which the adenine ring lies in a plane similar to that of adenine B of Ap_5A and stacks against the side chain of Gln-40 (Figure 4). However, the ribose moiety of 5′-ADP shows a ∼2.5 Å displacement and a ∼180° flip that leads to a significant difference in the alignment of the attached adenine.

The torsion angle of the N-glycosidic linkage of adenosine A (χ_A) places its adenine in the energetically favorable high-*anti* conformation in which the AC8 atom lies over the ribose ring (Table 5). This arrangement is highly similar to that seen in the EDN·3′,5′-ADP complex (*25*) and in structures of adenylic nucleotide inhibitors bound productively to the B_2 subsite of RNase A (*44*−*47*). The conformation of ribose A is somewhat unusual in that it adopts a 4′-*exo* conformation and its δ_A torsion angle lies in the +*sc* range. These features have precedents among free and protein-bound nucleotides (*54*) but are not typical of adenylic nucleotides bound to pancreatic ribonuclease superfamily members. For example, the furanose rings in the EDN·3′,5′-ADP, RNase A·3′,5′-ADP, and RNase A·d(CpA) complexes all adopt 2′-*endo* conformations and have δ angles in the +*ac* range (*25*, *44*, *47*). The torsion angles of adenosine B all lie within ranges commonly observed for free and protein-bound nucleotides, and the C2′-*endo* conformation adopted by ribose B is favored by protein-bound nucleotides.

Dinucleoside oligophosphates interact with many intra- and extracellular proteins of mammals (for reviews, see refs *55* and *56*). The interaction of dinucleoside pentaphosphates with one particular class of enzymes, the nucleoside monophosphate kinases (NMPKs), has been studied at high resolution (reviewed in ref *57*). These enzymes play essential roles in nucleotide metabolism and in the maintenance of cellular energy charge and are inhibited by dinucleoside pentaphosphates. There are close similarities in the ways in which these compounds bind to NMPKs from diverse organisms: in the crystal structures of Ap_5A bound to adenylate kinase from *Bacillus stearothermophilus* (PDB entry 1ZIN) (*58*), Ap_5U bound to uridylate-cytidylate kinase from *Dictyostelium discoideum* (PDB entry 1UKE) (*59*), and Ap_5T bound to human thymidylate kinase (PDB entry 1E2Q) (*60*), the pentaphosphate chain of the nucleotide adopts a relatively extended conformation. This contrasts sharply with the contorted conformation of Ap_5A when bound to EDN (Figure 5), and it would appear that the flexibility of the pentaphosphate chain plays a significant role in the precocious nature of these compounds.

DISCUSSION

Strength of Inhibition. The inhibition constants for the adenylic inhibitors of EDN examined in this work have been determined previously (*27*), as have those of the adenosine diphosphates 5′-ADP, 2′,5′-ADP, and 3′,5′-ADP (*25*). Hence, the crystallographic data presented here enable some rationalization of the structure−affinity relationships of the present inhibitors. It is acknowledged that this type of analysis can be enhanced by undertaking thermodynamic measurements that enable the calculation of both the enthalpic and entropic contributions to ligand binding.

The affinity of 5′-ATP for EDN (K_i = 21 μM) is very similar to that of the conventionally binding 3′,5′-ADP (K_i = 32 μM) and a few-fold greater than that of the *retro*-binding 5′-ADP (K_i = 92 μM). The EDN·5′-ATP structure indicates that 5′-ATP can bind in both fashions, although with modifications to each. The relatively high strength of the electron density for the polyphosphate moiety suggests that interactions at the P_1 subsite provide the main driving force for 5′-ATP binding, as appears to be the case for the binding of phosphorylated nucleotides to various members of the pancreatic ribonuclease family (*25*, *47*). Because the set of interactions between the observable nucleotide and the protein includes only interactions that are present in the EDN·3′,5′-ADP and EDN·5′-ADP structures, it appears that similarities in polyphosphate binding underlie the similar inhibition constants of these compounds. It is reasonable that the need to accommodate the extra phosphate group of

5′-ATP prevents the ordered binding of the adenosine moiety in the *retro* mode. However, we cannot readily explain why 5′-ADP does not behave like 5′-ATP in binding (albeit fractionally) in the conventional mode.

The affinity of Ap_3A for EDN ($K_i = 70\ \mu M$) is a few-fold less than that of 5′-ATP. Assuming, as above, that the binding of each is driven by the interactions of the polyphosphate moiety, the K_i values suggest that the polyphosphate interactions are less favorable with Ap_3A than with 5′-ATP. This is borne out by the observed conformational heterogeneity in the polyphosphate linker of Ap_3A; any deleterious effects on polyphosphate binding are likely to be compensated to some degree by favorable interactions at the B_2 subsite.

The affinity of Ap_4A for EDN ($K_i = 1.9\ \mu M$) is considerably greater (37-fold) than that of Ap_3A. A straightforward explanation is not provided by the structural data presented here. With each of these compounds, one adenine binds conventionally at the B_2 subsite, while the adjacent ribose and polyphosphate linker show conformational heterogeneity. The additional phosphate of Ap_4A appears to impart a little more order to the complexed polyphosphate moiety (Figure 2), and thus, there may be a difference in the strength of polyphosphate ligation. It is also possible that the longer linker alleviates unfavorable, transient interactions between adenosine B and the protein. Similar trends are seen for the inhibition of RNase A and angiogenin by Ap_3A and Ap_4A (*27*). However, no further structural or thermodynamic data are available for the complexes formed with these two proteins.

Ap_5A ($K_i = 0.37\ \mu M$) is the most avid inhibitor of this series. The high binding affinity can be attributed to multiple, well-defined interactions involving the α, *β*, and *δ* phosphates and to the binding of both adenosine moieties. Clearly, the additional length of the polyphosphate linker enables the formation of a set of new interactions and the alleviation of unfavorable interactions that may affect the binding of Ap_3A and Ap_4A.

Design of Improved EDN Inhibitors. The specific inhibition of pancreatic ribonuclease superfamily members holds considerable promise for the elucidation of their normal physiological roles and for the treatment of several human diseases (*17*, *18*). Guided by an EDN·Ap_5A structure at a resolution higher than that of any other protein·Np_nN complex determined to date, it may now be possible to design improved inhibitors of EDN.

Examination of the EDN surface using VOIDOO (*39*) indicates that there are no major cavities in the immediate vicinity of the RNA-binding site that can be exploited to enhance the binding of Ap_5A. Manual inspection of the areas immediately surrounding the ligand reveals several small clefts such as the nonpolar one formed by Leu-45, Tyr-108, and Leu-130 close to adenine A, into which additional groups could penetrate (Figure 3). In addition, a 3′ phosphate could be attached to ribose A with the intention of mimicking 3′,5′-ADP, where the corresponding group makes water-mediated interactions with Trp-10. The side chain of Trp-7 also overhangs this area and could be exploited by adding planar structures to the inhibitor to promote stacking interactions. However, wild-type EDN is C-mannosylated at Trp-7 (*61*), which may influence the role of this residue. It is also secreted in a number of differentially N-glycosylated forms (sugar attachment at Asn-17, -59, -65, -84, and -92) (*15*, *62*), which may affect inhibitor binding.

Because the B_1 subsite of EDN has a strong preference for pyrimidines, replacement of one adenine with a pyrimidine such as uridine may yield a compound that occupies both the B_1 and B_2 subsites. However, the sugar−phosphate connections in the dinucleoside polyphosphates studied here involve the 5′ oxygen at both ends of the chain, which is not the case in RNA. Consequently, the pyrimidine is likely to approach the B_1 subsite from a very different perspective and may never bind authentically.

The use of diadenosine polyphosphates *in vivo* is undesirable. First, the polyphosphate linkers of these compounds are cleaved readily by a variety of hydrolases and phosphodiesterases both outside and inside the cell, limiting their biological half-lives (*63*). This can, however, be overcome by replacement of some or all of the phosphate groups with nonhydrolyzable alternatives such as methylene phosphonates or fluorophosphonates (*64*). Second, the compounds are of limited use in cases where an intracellular action is required: the abundant phosphate groups impart a significant negative charge at physiological pH, preventing the compounds from readily penetrating cell membranes. The charges can be masked by derivatizing with bioreversible neutral groups, e.g., bis-pivaloyl-oxymethyl (bisPOM). Such derivatives are readily transformed to free phosphate forms inside various cell types, providing a potential "pro-drug" strategy (*65*). Third, the compounds occur naturally and bind to a broad range of proteins (*64*). They are found intracellularly, where they appear to be involved in cell-cycle regulation and can inhibit ATP-dependent enzyme reactions, and extracellularly, where they are purinoreceptor ligands and modulators (ref *56* and references therein). Therefore, efforts need to be made to tailor the specificity of the inhibitor toward EDN. The difference in conformation of the polyphosphate chain that results when Ap_5A binds to EDN and NMPKs (Figure 5) suggests one way of enhancing specificity, i.e., the introduction of additional bridging atoms to constrain the linker in a contorted conformation. Three-dimensional structures featuring diadenosine polyphosphates in complex with other proteins (including other ribonucleases) will be required to guide further specificity enhancement.

ACKNOWLEDGMENT

We thank the scientists at the Synchrotron Radiation Source, Daresbury (U.K.), for their help with X-ray data collection.

REFERENCES

1. Gleich, G. J., Kita, H., and Adolphson, C. R. (1995) Eosinophils, in *Samter's Immunologic Diseases*, 5th ed. (Unanue, E. R., Ed.) Vol. 1, pp 205−245, Little Brown and Co., Boston, MA.
2. Beintema, J. J., Schuller, C., Irie, M., and Carsana, A. (1988) Molecular evolution of the ribonuclease superfamily, *Prog. Biophys. Mol. Biol. 51*, 165−192.
3. Ackerman, S. J., Gleich, G. J., Loegering, D. A., Richardson, B. A., and Butterworth, A. E. (1985) Comparative toxicity of purified human eosinophil granule cationic proteins for schistosomula of *Schistosoma mansoni*, *Am. J. Trop. Med. Hyg. 34*, 735−745.
4. Lehrer, R. I., Szklarek, D., Barton, A., Ganz, T., Hamann, K. J., and Gleich, G. J. (1989) Antibacterial properties of eosinophil major basic protein and eosinophil cationic protein, *J. Immunol. 142*, 4428−4434.

5. Rosenberg, H. F., and Domachowske, J. B. (2001) Eosinophils, eosinophil ribonucleases, and their role in host defense against respiratory virus pathogens, *J. Leukocyte Biol. 70*, 691−698.
6. Yang, D., Rosenberg, H. F., Chen, Q., Dyer, K. D., Kurosaka, K., and Oppenheim, J. J. (2003) Eosinophil-derived neurotoxin (EDN), an antimicrobial protein with chemotactic activities for dendritic cells, *Blood 102*, 3396−3403.
7. Yang, D., Chen, Q., Rosenberg, H. F., Rybak, S. M., Newton, D. L., Wang, Z. Y., Fu, Q., Tchernev, V. T., Wang, M., Schweitzer, B., Kingsmore, S. F., Patel, D. D., Oppenheim, J. J., and Howard, O. M. Z. (2004) Human ribonuclease A superfamily members, eosinophil-derived neurotoxin and pancreatic ribonuclease, induce dendritic cell maturation and activation, *J. Immunol. 173*, 6134−6142.
8. Gleich, G. J. (2000) Mechanisms of eosinophil-associated inflammation, *J. Allergy Clin. Immunol. 105*, 651−663.
9. Robinson, D. S., Assoufi, B., Durham, S. R., and Kay, A. B. (1995) Eosinophil cationic protein (ECP) and eosinophil protein X (EPX) concentrations in serum and bronchial lavage fluid in asthma. Effect of prednisolone treatment, *Clin. Exp. Allergy 25*, 1118−1127.
10. Sedgwick, J. B., Calhoun, W. J., Gleich, G. J., Kita, H., Abrams, J. S., Schwartz, L. B., Volovitz, B., Ben-Yaakov, M., and Busse, W. W. (1991) Immediate and late airway response of allergic rhinitis patients to segmental antigen challenge. Characterization of eosinophil and mast cell mediators, *Am. Rev. Respir. Dis. 144*, 1274−1281.
11. Levy, A. M., Gleich, G. J., Sandborn, W. J., Tremaine, W. J., Steiner, B. L., and Phillips, S. F. (1997) Increased eosinophil granule proteins in gut lavage fluid from patients with inflammatory bowel disease, *Mayo Clin. Proc. 72*, 117−123.
12. Breuer, K., Kapp, A., and Werfel, T. (2001) Urine eosinophil protein X (EPX) is an *in vitro* parameter of inflammation in atopic dermatitis of the adult age, *Allergy 56*, 780−784.
13. Bonini, S., Magrini, L., Rotiroti, G., Lambiase, A., Tomassini, M., Rumi, C., and Bonini, S. (1997) The eosinophil and the eye, *Allergy 52*, 44−47.
14. Newton, D. L., Walbridge, S. M., Mikulski, S. M., Ardelt, W., Shogen, K., Ackerman, S. J., Rybak, S. M., and Youle, R. J. (1994) Toxicity of an antitumor ribonuclease to Purkinje neurons, *J. Neurosci. 14*, 538−544.
15. Gleich, G. J., Loegering, D. A., Bell, M. P., Checkel, J. L., Ackerman, S. J., and McKean, D. J. (1986) Biochemical and functional similarities between human eosinophil-derived neurotoxin and eosinophil cationic protein: Homology with ribonuclease, *Proc. Natl. Acad. Sci. U.S.A. 83*, 3146−3150.
16. Sorrentino, S., Glitz, D. G., Hamann, K. J., Loegering, D. A., Checkel, J. L., and Gleich, G. J. (1992) Eosinophil-derived neurotoxin and human liver ribonuclease. Identity of structure and linkage of neurotoxicity to nuclease activity, *J. Biol. Chem. 267*, 14859−14865.
17. Russo, A., Acharya, K. R., and Shapiro, R. (2001) Small molecule inhibitors of RNase A and related enzymes, *Methods Enzymol. 341*, 629−648.
18. Kumar, K., Brady, M., and Shapiro, R. (2004) Selective abolition of pancreatic RNase binding to its inhibitor protein, *Proc. Natl. Acad. Sci. U.S.A. 101*, 53−58.
19. Richards, F. M., and Wyckoff, H. W. (1971) Bovine pancreatic ribonuclease, in *The Enzymes*, 3rd ed. (Boyer, P. D., Ed.) Vol. 4, pp 647−806, Academic Press, New York.
20. Nogués, M. V., Moussaoui, M., Boix, E., Vilanova, M., Ribó, M., and Cuchillo, C. M. (1998) The contribution of noncatalytic phosphate-binding subsites to the mechanism of bovine pancreatic ribonuclease A, *Cell. Mol. Life Sci. 54*, 766−774.
21. Fisher, B. M., Grilley, J. E., and Raines, R. T. (1998) A new remote subsite in ribonuclease A, *J. Biol. Chem. 273*, 34134−34138.
22. Shapiro, R., and Vallee, B. L. (1991) Interaction of human placental ribonuclease with placental ribonuclease inhibitor, *Biochemistry 30*, 2246−2255.
23. Harper, J. W., and Vallee, B. L. (1989) A covalent angiogenin/ribonuclease hybrid with a fourth disulfide bond generated by regional mutagenesis, *Biochemistry 28*, 1875−1884.
24. Mosimann, S. C., Newton, D. L., Youle, R. J., and James, M. N. (1996) X-ray crystallographic structure of recombinant eosinophil-derived neurotoxin at 1.83 Å resolution, *J. Mol. Biol. 260*, 540−552.
25. Leonidas, D. D., Boix, E., Prill, R., Suzuki, M., Turton, R., Minson, K., Swaminathan, G. J., Youle, R. J., and Acharya, K. R. (2001) Mapping the ribonucleolytic active site of eosinophil-derived neurotoxin (EDN). High-resolution crystal structures of EDN complexes with adenylic nucleotide inhibitors, *J. Biol. Chem. 276*, 15009−15017.
26. Swaminathan, G. J., Holloway, D. E., Veluraja, K., and Acharya, K. R. (2002) Atomic resolution (0.98 Å) structure of eosinophil-derived neurotoxin, *Biochemistry 41*, 3341−3352.
27. Kumar, K., Jenkins, J. L., Jardine, A. M., and Shapiro, R. (2003) Inhibition of mammalian ribonucleases by endogenous adenosine dinucleotides, *Biochem. Biophys. Res. Commun. 300*, 81−86.
28. Boix, E., Nikolovski, Z., Moiseyev, G. P., Rosenberg, H. F., Cuchillo, C. M., and Nogués, M. V. (1999) Kinetic and product distribution analysis of human eosinophil cationic protein indicates a subsite arrangement that favours exonuclease-type activity, *J. Biol. Chem. 274*, 15605−15614.
29. Otwinowski, Z., and Minor, W. (1997) Processing of X-ray diffraction data collected in oscillation mode, *Methods Enzymol. 276*, 307−326.
30. Vagin, A., and Teplyakov, A. (1997) MOLREP: An automated program for molecular replacement, *J. Appl. Crystallogr. 30*, 1022−1025.
31. Bailey, S. (1994) The CCP4 suite: Programs for protein crystallography, *Acta Crystallogr., Sect. D: Biol. Crystallogr. 50*, 760−763.
32. Brünger, A. T., Adams, P. D., Clore, G. M., DeLano, W. L., Gros, P., GrosseKunstleve, R. W., Jiang, J. S., Kuszewski, J., Nilges, M., Pannu, N. S., Read, R. J., Rice, L. M., Simonson, T., and Warren, G. L. (1998) Crystallography and NMR system: A new software suite for macromolecular structure determination, *Acta Crystallogr., Sect. D: Biol. Crystallogr. 54*, 905−921.
33. Brünger, A. T. (1992) The free *R*-value: A novel statistical quantity for assessing the accuracy of crystal structures, *Nature 355*, 472−474.
34. Jones, T. A., Zou, J. Y., Cowan, S. W., and Kjeldgaard, M. (1991) Improved methods for binding proetin models in electron density maps and the location of errors in these models, *Acta Crystallogr., Sect. A: Found. Crystallogr. 47*, 109−110.
35. Sheldrick, G. M. (1997) SHELXL: High-resolution refinement, *Methods Enzymol. 277*, 319−343.
36. Merritt, E. A. (1999) Expanding the model: Anisotropic displacement parameters in protein structure refinement, *Acta Crystallogr., Sect. D: Biol. Crystallogr. 55*, 1109−1117.
37. Laskowski, R. A., MacArthur, M. W., Moss, D. S., and Thornton, J. M. (1993) PROCHECK: A program to check the stereochemical quality of protein structures, *J. Appl. Crystallogr. 26*, 283−291.
38. McDonald, I. K., and Thornton, J. M. (1994) Satisfying hydrogen bonding potential in proteins, *J. Mol. Biol. 238*, 777−793.
39. Kleywegt, G. J., and Jones, T. A. (1994) Detection, delineation, measurement and display of cavities in macromolecular structures, *Acta Crystallogr., Sect. D: Biol. Crystallogr. 50*, 178−185.
40. Leonidas, D. D., Shapiro, R., Allen, S. C., Subbarao, G. V., Veluraja, K., and Acharya, K. R. (1999) Refined crystal structures of native human angiogenin and two active site variants: Implications for the unique functional properties of an enzyme involved in neovascularisation during tumour growth, *J. Mol. Biol. 285*, 1209−1233.
41. Boix, E., Leonidas, D. D., Nikolovski, Z., Nogués, M. V., Cuchillo, C. M., and Acharya, K. R. (1999) Crystal structure of eosinophil cationic protein at 2.4 Å resolution, *Biochemistry 38*, 16794−16801.
42. Aguilar, C. F., Thomas, P. J., Moss, D. S., Mills, A., and Palmer, R. A. (1991) Novel non-productively bound ribonuclease inhibitor complexes—High-resolution X-ray refinement studies on the binding of RNase-A to cytidylyl-2′,5′-guanosine (2′,5′CpG) and deoxycytidylyl-3′,5′-guanosine (3′,5′dCpdG), *Biochim. Biophys. Acta 1118*, 6−20.
43. Borkakoti, N., Moss, D. M., and Palmer, R. A. (1982) Ribonuclease-A: Least-squares refinement of the structure at 1.45 Å resolution, *Acta Crystallogr., Sect. B: Struct. Sci. 38*, 2210−2217.
44. Zegers, I., Maes, D., Dao-Thi, M.-H., Poortmans, F., Palmer, R., and Wyns, L. (1994) The structures of RNase A complexed with 3′-CMP and d(CpA): Active site conformation and conserved water molecules, *Protein Sci. 3*, 2322−2339.
45. Fontecilla-Camps, J. C., de Llorens, R., le Du, M. H., and Cuchillo, C. M. (1994) Crystal structure of ribonuclease A·d(ApTpApApG) complex. Direct evidence for extended substrate recognition, *J. Biol. Chem. 269*, 21526−21531.
46. Toiron, C., Gonzalez, C., Bruix, M., and Rico, M. (1996) Three-dimensional structure of the complexes of ribonuclease A with

2′,5′-CpA and 3′,5′−d(CpA) in aqueous solution, as obtained by NMR and restrained molecular dynamics, *Protein Sci. 5*, 1633−1647.
47. Leonidas, D. D., Chavali, G. B., Oikonomakos, N. G., Chrysina, E. D., Kosmopoulou, M. N., Vlassi, M., Frankling, C., and Acharya, K. R. (2003) High-resolution crystal structures of ribonuclease A complexed with adenylic and uridylic nucleotide inhibitors. Implications for structure-based design of ribonucleolytic inhibitors, *Protein Sci. 12*, 2559−2574.
48. McPherson, A., Brayer, G. D., and Morrison, R. D. (1986) Crystal structure of RNase A complexed with $d(pA)_4$, *J. Mol. Biol. 189*, 305−327.
49. McPherson, A., Brayer, G., Cascio, D., and Williams, R. (1986) The mechanism of binding of a polynucleotide chain to pancreatic ribonuclease, *Science 232*, 765−768.
50. Aguilar, C. F., Thomas, P. J., Mills, A., Moss, D. S., and Palmer, R. A. (1992) Newly observed binding mode in pancreatic ribonuclease, *J. Mol. Biol. 224*, 265−267.
51. Lisgarten, J. N., Maes, D., Wyns, L., Aguilar, C. F., and Palmer, R. A. (1995) Structure of the crystalline complex of deoxycytidylyl-3′,5′-guanosine (3′,5′-dCpdG) cocrystallized with ribonuclease at 1.9 Å resolution, *Acta Crystallogr., Sect. D: Biol. Crystallogr. 51*, 761−771.
52. Vitagliano, L., Adinolfi, S., Sica, F., Merlino, A., Zagari, A., and Mazzarella, L. (1999) A potential allosteric subsite generated by domain swapping in bovine seminal ribonuclease, *J. Mol. Biol. 293*, 569−577.
53. Vitagliano, L., Merlino, A., Zagari, A., and Mazzarella, L. (2000) Productive and nonproductive binding to ribonuclease A: X-ray structure of two complexes with uridylyl(2′,5′)guanosine, *Protein Sci. 9*, 1217−1225.
54. Moodie, S. L., and Thornton, J. M. (1993) A study into the effects of protein binding on nucleotide conformation, *Nucleic Acids Res. 21*, 1369−1380.
55. Baxi, M. D., and Vishwanatha, J. K. (1995) Diadenosine polyphosphates: Their biological and pharmacological significance, *J. Pharmacol. Toxicol. Methods 33*, 121−128.
56. McLennan, A. G. (2000) Dinucleoside polyphosphates—Friend or foe? *Pharmacol. Ther. 87*, 73−89.
57. Yan, H., and Tsai, M.-D. (1999) Nucleoside monophosphate kinases: Structure, mechanism, and substrate specificity, *Adv. Enzymol. Relat. Areas Mol. Biol. 73*, 103−134.
58. Berry, M. B., and Phillips, G. N., Jr. (1998) Crystal structures of *Bacillus stearothermophilus* adenylate kinase with bound Ap_5A, Mg^{2+} Ap_5A, and Mn^{2+} Ap_5A reveal an intermediate lid position and six coordinate octahedral geometry for bound Mg^{2+} and Mn^{2+}, *Proteins 32*, 276−288.
59. Scheffzek, K., Kliche, W., Wiesmuller, L., and Reinstein, J. (1996) Crystal structure of the complex of UMP/CMP kinase from *Dictyostelium discoideum* and the bisubstrate inhibitor P1-(5′-adenosyl) P5-(5′-uridyl) pentaphosphate (Up_5A) and Mg^{2+} at 2.2 Å: Implications for water-mediated specificity, *Biochemistry 35*, 9716−9727.
60. Ostermann, N., Schlichting, I., Brundiers, R., Konrad, M., Reinstein, J., Veit, T., Goody, R. S., and Lavie, A. (2000) Insights into the phosphoryltransfer mechanism of human thymidylate kinase gained from crystal structures of enzyme complexes along the reaction coordinate, *Structure 8*, 629−642.
61. Löffler, A., Doucey, M.-A., Jansson, A. M., Müller, D. R., de Beer, T., Hess, D., Meldal, M., Richter, W. J., Vliegenthart, J. F. G., and Hofsteenge, J. (1996) Spectroscopic and protein chemical analyses demonstrate the presence of C-mannosylated tryptophan in intact human RNase 2 and its isoforms, *Biochemistry 35*, 12005−12014.
62. Beintema, J. J., Hofsteenge, J., Iwama, M., Morita, T., Ohgi, K., Irie, M., Sugiyama, R. H., Schieven, G. L., Dekker, C. A., and Glitz, D. G. (1988) Amino acid sequence of the nonsecretory ribonuclease of human urine, *Biochemistry 27*, 4530−4538.
63. Guranowski, A. (2003) Specific and nonspecific enzymes involved in the catabolism of mononucleoside and dinucleoside polyphosphates, *Pharmacol. Ther. 87*, 117−139.
64. Guranowski, A. (2003) Analogs of diadenosine tetraphosphate (Ap_4A), *Acta Biochim. Pol. 50*, 947−972.
65. Farquhar, D., Chen, R., and Khan, S. (1995) 5′-[4-(Pivaloyloxy)-1,3,2-dioxaphosphorinan-2-yl]-2′-deoxy-5-fluorouridine: A membrane-permeating prodrug of 5-fluoro-2′-deoxyuridylic acid (FdUMP), *J. Med. Chem. 38*, 488−495.
66. IUPAC−IUB Joint Commission on Biochemical Nomenclature (1983) Abbreviations and symbols for the description of conformations of polynucleotide chains, *Eur. J. Biochem. 131*, 9−15.
67. Altona, C., and Sundaralingam, M. (1972) Conformational analysis of the sugar ring in nucleosides and nucleotides. A new description using the concept of pseudorotation, *J. Am. Chem. Soc. 94*, 8205−8212.

BI0518592